On the X-ray spectra of luminous, inhomogeneous accretion flows

A. Merloni,[1]⋆ J. Malzac,[2] A. C. Fabian[3] and R. R. Ross[4]

[1]*Max-Planck-Institut für Astrophysik, Karl-Schwarzschild-Strasse 1, D-85741 Garching, Germany*
[2]*Centre d'Estude Spatiale des Rayonnements, CNRS-UPS 9, Avenue du Colonel Roche, 31028 Toulouse Cedex 4, France*
[3]*Institute of Astronomy, Madingley Road, Cambridge CB3 0HA*
[4]*Physics Department, College of the Holy Cross, Worcester, MA 01610, USA*

ABSTRACT

We discuss the expected X-ray spectral and variability properties of black hole accretion discs at high luminosity, under the hypothesis that radiation-pressure-dominated discs are subject to violent clumping instabilities and, as a result, have a highly inhomogeneous two-phase structure. After deriving the full accretion disc solutions explicitly in terms of the parameters of the model, we study their radiative properties both with a simple two-zone model, treatable analytically, and with radiative transfer simulations which account simultaneously for energy balance and Comptonization in the hot phase, together with reflection, reprocessing, ionization and thermal balance in the cold phase. We show that, if not only the density, but also the heating rate within these flows is inhomogeneous, then complex reflection-dominated spectra can be obtained for a high enough covering fraction of the cold phase. In general, large reflection components in the observed X-ray spectra should be associated with strong soft excesses, resulting from the combined emission of ionized atomic emission lines. The variability properties of such systems are such that, even when contributing to a large fraction of the hard X-ray spectrum, the reflection component is less variable than the power-law-like emission originating from the hot Comptonizing phase, in agreement with what is observed in many Narrow Line Seyfert 1 galaxies and bright Seyfert 1. Our model falls within the family of those trying to explain the complex X-ray spectra of bright AGN with ionized reflection, but presents an alternative, specific, physically motivated, geometrical set-up for the complex multiphase structure of the inner regions of near-Eddington accretion flows.

Key words: accretion, accretion discs – black hole physics.

1 INTRODUCTION

Black Hole systems, either in X-ray binaries (BHXRB) or in active galactic nuclei (AGN), when shining at luminosities close to the Eddington limit are thought to be powered by accretion through geometrically thin, optically thick discs, where angular momentum is transferred by the stresses due to magnetorotational instability (MRI; Balbus & Hawley 1991, 1998). From the observational point of view, the presence of such discs is inferred from the spectral properties of transient BHXRB at (or close to) the peak of their outburst luminosities (in the so-called high/very high/intermediate states, see e.g. Belloni 2004, or McClintock & Remillard 2006 for a different nomenclature, and references therein) and from the dominance of the quasi-thermal ultraviolet (UV) emission in bright quasars (see e.g. Malkan 1983; Laor 1990; Shang et al. 2005). According to the standard models (Shakura & Sunyaev 1973), such accretion discs

are radiatively efficient, as they are able to convert into radiation a sizeable fraction (between 6 and ∼40 per cent, depending on black hole spin) of the available gravitational energy of the accreting gas. Indeed, radiative efficiency estimates obtained by comparing the total supermassive black hole mass density in the local universe with the accretion power released by quasars and AGN suggest that this is probably the main mode of growth by accretion of supermassive black holes (see e.g. Fabian & Iwasawa 1999; Elvis, Risaliti & Zamorani 2002; Yu & Tremaine 2002; Marconi et al. 2004; Merloni, Rudnick & Di Matteo 2004). It is therefore clear that a good understanding of the accretion mechanism associated with near-Eddington sources can shed light on fundamental issues of black holes astrophysics.

Nonetheless, according to the above mentioned standard accretion disc solutions, such highly luminous discs should be radiation pressure dominated and therefore unstable to perturbations of both mass flow (Lightman & Eardley 1974) and heating rates (Shakura & Sunyaev 1976). Thus, it is not clear yet to what extent these standard solutions represent a realistic description of the observed systems. In

⋆E-mail: am@mpa-garching.mpg.de

recent years, both analytic works (Blaes & Socrates 2001, 2003) and simulations (Turner Stone & Sano 2002; Turner et al. 2003b; Turner 2004) have shown that magnetized, radiation-pressure-dominated accretion discs may be in fact subject to violent clumping instabilities if magnetic pressure exceeds gas pressure and photons are able to diffuse from compressed regions. Large density variations may also be caused by photon bubble instabilities (Gammie 1998), which may develop into a series of shocks propagating through the plasma (Begelman 2001, 2002; Turner et al. 2005). These instabilities may in turn have profound effects not only on the nature of the cooling mechanism of luminous discs, but also on their observational appearance (see e.g. Davis et al. 2004; Ballantyne, Turner & Blaes 2004), as we discuss in this work.

Radiative models for inhomogeneous, clumpy discs that explain the X-ray properties of accreting black holes have been proposed since long time. Most of the previous works were devoted to the study of the internal state of the cold clumps and on their radiative output (Guilbert & Rees 1988; Celotti, Fabian & Rees 1992; Collin-Souffrin et al. 1996; Kuncic, Celotti & Rees 1997). Krolik (1998) studied analytically the overall equilibrium of a clumpy two-phase accretion disc, while Malzac & Celotti (2002; hereafter MC02) studied numerically the Comptonization equilibrium between the cold clumps and the hot surrounding plasma and calculated the emitted X-ray spectrum.

In this paper, we explore in detail the consequences of the hypothesis that accretion flows close to the Eddington rate are indeed inhomogeneous. In particular, we present a detailed study of their expected X-ray spectral and variability properties, extending the results of MC02 both numerically and analytically. From the numerical point of view, we calculate the emerging spectrum from an inhomogeneous, two-phase, clumpy flow by coupling the non-linear Monte Carlo code of Malzac & Jourdain (2000), that calculates the Compton equilibrium between the cold and the hot phase, with the X-ray ionized reflection code of Ross & Fabian (1993, 2005), that accurately computes the reprocessed radiation in the cold phase. From the analytic point of view, we are able to show that a crucial factor in determining the broad-band spectral properties of an inhomogeneous flow is not only the amount of cold clouds/filaments pervading the hot plasma (as considered in all the previous studies cited above), but also the level of inhomogeneity of the *heating* in the hot phase itself. Indeed, we will demonstrate both analytically and numerically, the very important result that the more localized the heating is (as due to, e.g. a reconnection event), the more emerging spectra are dominated by reflection/reprocessing, as already suggested by Fabian et al. (2002).

In this paper, we will also show that a model for an accretion flow which is inhomogeneous both in its density and heating structure can explain many of the observed properties of black holes accreting at rates close to the Eddington one (e.g. bright QSOs and Narrow Line Seyfert galaxies). In particular, flows with varying degrees of inhomogeneity naturally produce little variability in the observed reflected component associated with large variations of the power-law continuum, and reflection-dominated spectra at the lowest-luminosity levels, in a strikingly similar fashion to what predicted by the so-called light bending model (Miniutti & Fabian 2004). Similarly, such a configuration naturally produces multiple reflections of the X-ray emission that can enhance the broad emission and absorption features in the observed spectra (Collin-Souffrin et al. 1996; Ross, Fabian & Ballantyne 2002).

The paper is structured as follows. In Section 2 we first introduce our simple toy model for a clumpy, two-phase medium with inhomogeneous heating. As this model is treatable analytically, we are able to discuss the main expected properties (spectra and variability) over a wide area of the parameter space. In Section 3 we then discuss our numerical simulations, while in Section 4 we discuss the relevance of our results for observations of high accretion rate BHXRB and AGN and their implications for models of accretion flows. Finally, we draw our conclusions in Section 5. In addition, we have developed in Appendix A a full inhomogeneous accretion disc model based on the picture discussed in Section 2 in which the dependence of our model parameters on radius, black hole mass and accretion rate is made explicit.

2 A SIMPLE TOY MODEL

In order to gain insight into the main expected observable properties of inhomogeneous discs, we introduce first a simple, yet motivated, idealized model, which is tractable analytically. In Appendix A, instead, we present a full inhomogeneous accretion disc model, closely following the ideas of Krolik (1998), with the aim of constraining the values and the scalings of the parameters we introduce in order to describe the disc inhomogeneity (see below).

Let us consider a sphere of hot plasma with uniform density and radius H, pervaded by small lumps of cold matter randomly distributed throughout the hot phase. Such a system may represent the inner region of an accretion flow (with $H \approx$ few Schwarzschild radii, R_S), or a patch of the accretion disc itself in the radiation-pressure-dominated region, where clumping instability is at work (with $H \approx$ disc scaleheight, see Appendix A). Then we can write $H = r R_S = 3 \times 10^{12} m_7 r_0$ cm, where m_7 is the mass of the central black hole in units of $10^7 \, M_\odot$, and $r_0 = r/1$.[1] As already discussed in MC02, the lack of strong absorption features in the X-ray spectra of accreting black holes suggests that any putative cold clump of matter immersed in the hot plasma should be optically (Thomson) thick (see also, Kuncic et al. 1997), with zero transmission. Thus we consider clouds with column densities $\gtrsim 10^{25} \, \text{cm}^{-2}$, which implies a density $n_{\text{cl}} \gtrsim 3.3 \times 10^{13} (m_7 \epsilon_{-1} r_0)^{-1} \, \text{cm}^{-3}$, where we have introduced the parameter $\epsilon = 0.1 \epsilon_{-1}$, the ratio of the cloud size to the system size H.

We assume that the whole system is in radiative equilibrium. However, differently from MC02, we allow the heating to be localized in a small region, rather than diffused throughout the hot phase. For simplicity, we assume that the heating of the hot plasma takes place only in an inner concentric sphere of radius $Z \equiv hH$ (see Fig. 1), where a power L_h is deposited. The outer zone can therefore be viewed as a passive reprocessor (see Appendix B). In our idealized model the injected power eventually escapes the system as three different kinds of radiation:

$$L_h = L_{\text{UV}} + L_C + L_R, \tag{1}$$

respectively, the UV/soft X-ray reprocessed luminosity, the Comptonized (power-law-like) luminosity and the reflected luminosity. In our calculation, we also assume that the UV/soft X-ray radiation reprocessed by the clouds is the only source of soft photons (no internal dissipation in the cold clumps, see e.g. the discussion in Collin-Souffrin et al. 1996, or Malzac 2001).

If the clouds are sufficiently small, we can use an effective cloud optical depth, τ_B, as the main parameter controlling the amount of cold matter. This is defined in such a way that a photon crossing the hot plasma has a probability $1 - e^{-\tau_B}$ of intercepting a cloud. The second parameter that affects the emerging spectrum

---

[1] Throughout the paper we use the representation $A_x = A/10^x$.
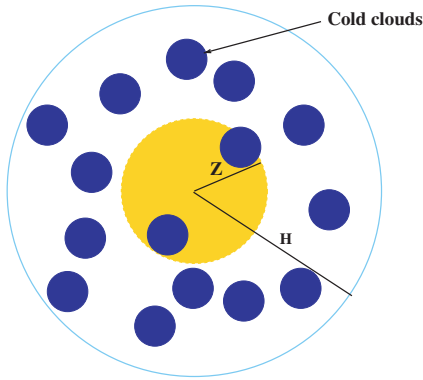
Figure 1. A simple two-zone model for an inhomogeneous accretion flow. The hot plasma emitting the hard X-rays is pervaded by small clouds of dense matter, optically thick to Thomson scattering. Both cold clumps and the hot plasma are uniformly distributed, but the heating is only concentrated inside the inner sphere of radius $Z \equiv hH$. The system is assumed to be in radiative equilibrium.

is the optical depth to Thomson scattering of the hot plasma, τ_T. Comptonization models for the X-ray emission from compact objects typically constrain the hot plasma Thomson optical depth $\tau_T \sim 1$ (see e.g. Zdziarski 1999). This is also consistent with the upper and lower limits on τ_T derived by Krolik (1998) from the thermal and evaporative equilibrium of a clumpy disc.

A rough order of magnitude estimate of the expected ionization parameter can be derived as follows: radiatively heated clouds with no internal dissipation, if dense enough (as we are assuming here, see also Collin-Souffrin et al. 1996; Kuncic et al. 1997), will re-emit the absorbed flux as a blackbody with typical energy $kT_{bb} \simeq 30 L_{44}^{1/4} (m_7 r_0)^{-1/2}$ eV, where L is the bolometric luminosity of the system and the weak dependence on the albedo has been neglected. Then, assuming that in the hot phase gas pressure dominates over radiation pressure (an assumption that can be verified a posteriori, see details in Appendix A), thermal pressure balance between the cold clouds and the hot phase implies that

$$n_{cl} \simeq 3.3 \times 10^{15} \left(\frac{\tau_T}{1} \right) \left(\frac{kT_{hot}}{100\,\text{keV}} \right) (m_7 r_0)^{-1/2} L_{44}^{-1/4}\ \text{cm}^{-3} \quad (2)$$

Therefore, the typical ionization parameter[2]

$$\xi = \frac{4\pi F}{n_{cl}} \simeq 3.5 \times 10^3 L_{44}^{5/4} (m_7 r_0)^{-3/2} \left(\frac{\tau_T}{1} \right)^{-1} \left(\frac{kT_{hot}}{100\,\text{keV}} \right)^{-1}. \quad (3)$$

It is worth stressing, however, that in the inhomogeneous heating model we are discussing, a range of ionization parameters is expected, given the sensitivity of ξ to the actual geometry of the system. The above equation has to be considered just an order of magnitude estimate. Indeed, the above estimates are consistent with the values obtained with the full disc modelling outlined in Appendix A, where the explicit scalings of cloud density, temperature and ionization parameters with accretion disc radius, black mass and accretion rate are presented. In the following (see Section 3), we will explore the effects of changing the value of ξ on the spectra emerging from our inhomogeneous flow.

[2]Here, as in the remaining of the paper, the ionization parameter will be expressed in erg cm s^{-1}.

The other parameters needed to compute the emerging radiation intensity are the energy and angle-integrated single-reflection albedos for a Comptonized and reflection spectrum, a and a_R, respectively. Malzac, Dumont & Mouchet (2005) have shown that, when the reprocessed spectrum is computed self-consistently the X-ray albedo is a strong function of the ionization parameter and of the spectrum of the illuminating radiation. Moreover, multiple reflections start to become important for $\tau_B \sim 1$. In a simple one-zone model, the net albedo produced by multiple reflections should be approximately given by (equation 2 of Ross et al. 2002):

$$a_{net} = \frac{\varepsilon a}{1 - (1 - \varepsilon)a}, \quad (4)$$

where ε is the escape probability for a reflected photon and a is the albedo for a single reflection by the material. We should expect that, whenever heating is inhomogeneous the cold clumps in the inner heated zone and in the outer one will not only be exposed to illuminating radiation with different spectra, but also experience different numbers of multiple reflections. Thus, it is plausible to conceive that in general ε will not be identical to $\exp(-\tau_B)$ as would be in a simple one zone model. For the sake of simplicity, and because the main purpose of the toy model discussed here is to give a coherent qualitative picture of the properties of inhomogeneous flows, we have chosen to calibrate the net albedo directly on the simulated spectra that will be presented in Section 3. To a very high degree of accuracy, we find that, for a ionization parameter of $\xi = 300$, the net albedo is a function of the optical depth of the cold clumps only, and can be expressed with a similar expression by replacing $\varepsilon = \exp(-\tau_B/1.43)$, with $a = 0.36$ (see also Fig. 7). The reflected radiation can itself be reflected many times for the most extremely inhomogeneous discs. Also for its albedo we have used the expression (4) with $\varepsilon = \exp(-\tau_B/1.82)$, with $a_R = 0.4$. This latter value is also consistent with the Monte Carlo simulations of Malzac (2001), where the albedo for a typical reflection spectrum illuminating neutral matter was computed. We have also verified that assuming an increased albedo of $a_R = 0.6$ to account for the effects of ionization have negligible effects on the final results of our analytic two-zone model.

We can then proceed as in Section 4 of MC02 and solve for the three different luminosities L_{UV}, L_C and L_R (and the corresponding reflection fraction R) making use of the analytic approximations for the corresponding photon escape probability calculated from Monte Carlo simulations (see equations A3 and A5 in MC02). We keep the heating rate, L_h, fixed and explore the parameter space spanned by $0.1 < \tau_B < 8$ and $0.05 < h < 0.9$. Details of the analytic calculation of the emerging luminosities in this two-zone model are given in the Appendix B. Once the soft and the Comptonized luminosities are found, we determine the spectral shape of the X-ray emission by calibrating the power-law index Γ with the numerical simulations (see below), where the power law index of the Comptonized emission is calculated by fitting the emergent spectra with the PEXRAV model in the 2–30 keV range. Apart from a very weak dependence on the heating inhomogeneity parameter, h, the power-law index depends only logarithmically on τ_B, with the spectrum being softer for larger cold clouds column densities. From the analysis of the results of the simulations, we derive the following phenomenological expression for the power-law index as a function of τ_B: $\Gamma \simeq 2 + 0.4 \log \tau_B$.

Fig. 2 shows the emerging luminosities as coloured contours in the two-dimensional parameter space (τ_B, h), for a Thomson optical depth of the hot phase $\tau_T = 1$. Shown are the relative intensities (normalized to the total heating rate L_h) of the X-ray Comptonized luminosity (L_C, upper left-hand panels), of the reflected luminos-
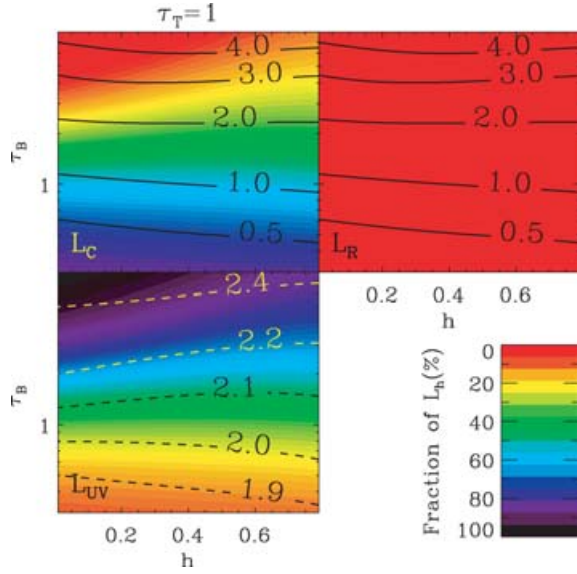
Figure 2. The relative intensity of the emerging hard X-ray Comptonized (L_C, upper left-hand panel), reprocessed UV (L_{UV}, lower left-hand panel), and reflected (L_R, upper right-hand panel) luminosities is plotted as colour-coded contours in the (τ_B, h) plane. Superimposed on them, in the two upper panels are the contours of constant reflection fraction (solid lines), ranging from $R = 0.5$ to $R = 4$, while in the lower panel we plot the contours (dashed lines) of constant power-law indexes Γ, from 1.9 to 2.4. The optical depth of the hot phase is assumed to be unity $\tau_T = 1$

ity (L_R, upper right-hand panels) and of the reprocessed UV/soft X-ray one (L_{UV}, lower left-hand panels). Superimposed on them, in the two upper panels are the contours of constant reflection fraction, defined as $R = L_R/(a_{net}L_X)$, where $L_X \equiv L_C(E > 1 \text{ keV})$ is the Comptonized luminosity emerging above 1 keV. This has been calculated analytically from L_C assuming that the Comptonized emission is power law with index Γ extending from $kT_{bb} = 50 \text{ eV}$ up to an energy corresponding to the temperature of the hot electrons $\Theta \equiv kT_{hot}/(m_e c^2) \approx (3/19)/[(\Gamma - 1)\tau_T^{4/5}]$ (Wardziński & Zdziarski 2000). In the lower panel we plot the contours of constant power-law spectral index, Γ.

As expected, the reflection fraction R increases with τ_B, as does the relative intensity of the soft reprocessed emission: the larger the filling factor of the cold component, the more reflection dominated the emerging spectrum will be. In general, large reflection fractions are always expected when the reprocessed component is strong compared to the direct Comptonized X-ray emission.

The relative intensity of the soft reprocessed luminosity, L_{UV}, is larger in the centrally heated case than in the uniformly heated case, if τ_B is large. As a result, for large enough τ_B and localized heating (i.e. in the upper left-hand corner of the plots shown in Fig. 2), the X-ray continuum power law is dominated by the reflection component and by the thermal reprocessed emission.

2.1 On the variability of the reflection component

One more interesting fact emerges from the study of this simple two-zone toy model. As can be seen in Fig. 2, the reflected luminosity L_R does not vary as much as L_X and L_{UV} across the explored region of the parameter space, at least as long as τ_B is smaller than ∼2 (note that the colour scale of Fig. 2 is linear). In fact, the reflected luminosity L_R has a broad maximum almost coincident with the locus of $R \approx 1$. To make this clearer, we have plotted in Fig. 3
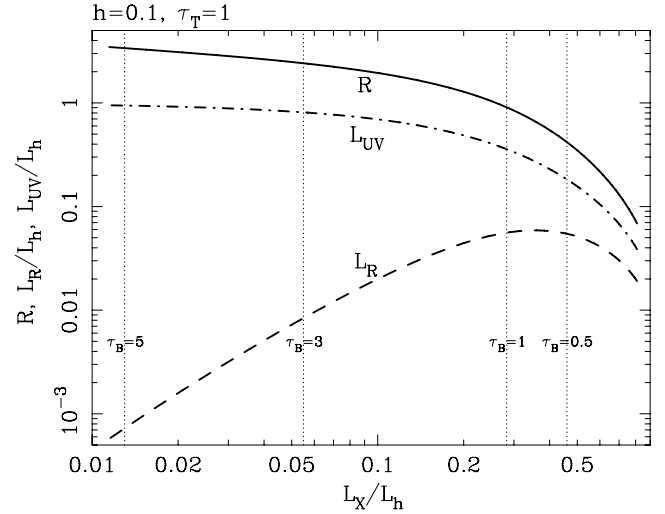

Figure 3. The relative intensity of the reflection component (R, solid line), of the reprocessed UV (L_{UV}, dot–dashed line) and reflected (L_R, dashed line) luminosities are plotted as functions of the emergent X-ray (Comptonized power-law) luminosity above 1 keV (L_X) for a varying cloud optical depth τ_B. All luminosities are renormalized by the total heating rate L_h, which is here assumed to be concentrated in an inner sphere of radius $h = 0.1$. The vertical dotted lines mark the X-ray luminosities corresponding to $\tau_B = 0.5, 1, 3, 5$.

the reflected luminosity, the soft reprocessed luminosity and the reflection fraction as a function of the X-ray (Comptonized) luminosity above 1 keV for the case of inhomogeneous heating $h = 0.1$ and $\tau_T = 1$ (those are also the values of the parameters adopted in our numerical simulations of Section 3 below). The fact that the reflected luminosity has a maximum, implies that large variations of the emergent X-ray luminosity, L_X, associated with changes in the cold clump integrated optical depth correspond to only modest variations of the reflection component, at least as long as $L_X/L_h \gtrsim 0.05$. On the other hand, for low values of the Comptonized X-ray luminosity, the reflected luminosity correlates with L_X, while at high L_X, the trend is the opposite.

This global behaviour of L_R versus L_X is analogous to that of the so-called 'light bending' model (Miniutti & Fabian 2004), which has been previously invoked to explain the variability properties of the continuum and of the iron line in a number of Narrow Line Seyfert 1 (NLS1) galaxies and galactic black holes in the very high state (see e.g. Miniutti et al. 2003; Fabian et al. 2004; Miniutti, Fabian & Miller 2004; Rossi et al. 2005). In particular, the defining property of the reflected luminosity to show a broad maximum as a function of the emerging X-ray (Comptonized) one is a common characteristic of both models. We will return to this similarity later on.

We have explored the variability property of our simple toy model in greater detail. In order to do so, we have computed the fractional variability σ_i of each spectral component ($i = $ X, UV, R), associated with variations $\delta \log \tau_B$, $\delta \log h$ of the cold clouds optical depth and of the inner heated region size, respectively:

$$\sigma_i(\delta \log \tau_B, \delta \log h) \equiv \left| \frac{\partial \log L_i}{\partial \log \tau_B} \right| \delta \log \tau_B + \left| \frac{\partial \log L_i}{\partial \log h} \right| \delta \log h. \quad (5)$$

Fig. 4 shows as contour plots the fractional variability levels of the three components calculated for $\delta \log \tau_B = \delta \log h = 10$ per cent. The fractional variability level of the X-ray emission can thus be relatively high (up to ∼50 per cent for $\tau_B \sim 2$) even for relatively small variations of the total optical depth. According to
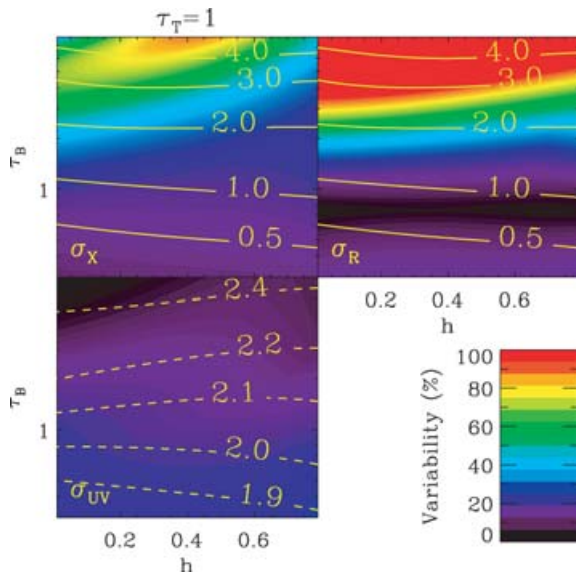
Figure 4. The total variability fraction, associated with variations of 10 per cent of τ_B and $h = Z/H$, of Comptonized X-rays emission above 1 keV (σ_X, upper left-hand panel), reprocessed UV (σ_{UV}, lower left-hand panel), and reflected (σ_R, upper right-hand panel) luminosities is plotted as colour-coded contours in the (τ_B, h) plane. Superimposed on them, in the two upper panels are the contours of constant reflection fraction (solid lines), ranging from $R = 0.5$ to 4, while in the lower panel we plot the contours (dashed lines) of constant power-law indexes Γ, from 1.9 to 2.4, which are the same as in Fig. 2.

our simple toy model of spherical clouds in a spherical volume, the total number of clouds, N, is related to the cold phase optical depth by $\tau_B = (3/4)N\epsilon^2$. The total number of clouds will have a dispersion around its mean value of $\sim\sqrt{N}$, so that $\Delta\tau_B/\tau_B = 0.1$ corresponds to $N \sim 100$ and $\epsilon \sim 0.11\sqrt{\tau_B}$. Interestingly, one obtains a similar constrain on the cloud size from considering thermal equilibrium in the presence of heat conduction (see Krolik 1998, equation 5): $\epsilon \simeq 0.2\, \tau_T^{-1}\, (kT_{hot}/100\,\mathrm{keV})^{3/2}$.

Overall, the fractional variability of L_X is higher if the reflection fraction R is high. For $\tau_B \lesssim 2$, and $R < 2$, the variability of the Comptonized emission, σ_X, is more than twice that of the UV/soft X-ray and reflected components. For even lower values of the cold phase optical depth $\tau_B \lesssim 0.5$, and correspondingly lower reflection fractions, the amount of variability is comparable in both hard and soft, reprocessed, components, while for the opposite extreme case of very large τ_B (i.e. for the case in which most of the X-ray and reflected emission is hidden from the view), the reflection component at high energies will vary most dramatically, while the UV/soft X-ray emission should be almost constant, with the Comptonized power-law emission varying by as much as 60–70 per cent.[3]

The direct analogy with the light bending model presented above lends itself to a simple geometrical explanation. In the more general framework of two-phase models for the X-ray spectra of accreting black holes, the main spectral and variability properties are determined by the radiative feedback between the hot and the cold phases.

---

[3]Obviously, it should always be kept in mind that we are here considering only the variability induced by structural/geometrical changes at fixed total heating rate L_h. One should naturally expect, in a realistic situation, that the heating rate is also variable on a dynamical time-scale, and its variations should contribute to the observed overall variability.

Such feedback is strongly dependent on the geometry (and on the topology) of the two phases and, in particular, on the sky covering fraction of the cold phase as seen by the hot, Comptonizing medium. Reflection dominated spectra are expected when the cold phase intercepts most of the photons coming from the hot phase. This, in the light bending model, is achieved via general relativistic (GR) effects, while here it is a result of the clumpy and inhomogeneous nature of the inner disc.

In more general terms, one can define as 'open' any geometry in which the hot, X-ray emitting plasma is photon starved (i.e. patchy coronae, inner ADAF plus outer discs etc.). Such a geometry will produce hard X-ray spectra, little soft thermal emission and weak reflection component (see e.g. the simple model of Zdziarski, Lubiński & Smith 1999). On the other hand, a 'closed' geometry will instead correspond to a very large covering fraction of the cold phase, with associated strong soft emission, softer spectra and strong reflection fraction (Collin-Souffrin et al. 1996). Such a geometry corresponds, observationally, to the highly accreting black holes. Whether this is due predominantly to strong GR effects as expected from centrally concentrated coronae atop a cold, thin disc in the immediate vicinity of the black event horizon, or to the more mundane inhomogeneous structure of a radiation-pressure-dominated disc, remains to be tested with accurate spectral modelling.

Is it possible to discriminate between these two scenarios for a 'closed' geometry? In principle, the relativistic blurring induced by the differential rotation of the inner disc should always be taken into account when fitting observed spectra. In the original light bending model, where the illuminating source is a point-like source above a standard geometrically thin disc, the ratio of the reflected component to the power-law continuum is determined by the same effects that determine the shape of the relativistic lines, while if the disc is truly inhomogeneous, the two effects can be decoupled. Therefore, simultaneous spectroscopic studies of relativistically blurred emission lines and of the broad-band continuum and variability could be effectively used to discriminated between a pure light bending model and a clumpy disc. Detailed predictions for the latter, however, require the combination of sophisticated MHD and radiative transfer simulations.

3 NUMERICAL SIMULATIONS

The toy model presented in Section 2 provides important qualitative predictions regarding the strength and variability of the different spectral components emerging from a clumpy accretion flow. In this section, we perform detailed radiative transfer calculations to investigate quantitatively the shape of the predicted spectra. These calculations account simultaneously for energy balance and Comptonization in the hot phase, together with reflection, reprocessing, ionization and thermal balance in the cold phase. The radiative processes in the hot gas are simulated using the non-linear Monte Carlo code of Malzac & Jourdain (2000), the reprocessed radiation from the cold clouds is computed using the photoionization code of Ross & Fabian (1993, 2005). The results of each code are used as input for the other code and self-consistency is achieved by multiple iterations as described in Malzac et al. (2005).

3.1 Set-up

The geometry we consider for the purpose of our numerical simulations differs from that of the simple analytical model presented in Section 2. The basic idea behind our calculations is to study the observed spectra emerging from a clumpy accretion flow in which

the heating is localized. Thus, the schematic two-zone toy model discussed in Section 2 represents here a patch of the accretion disc, with $H \sim$ disc scaleheight (spherical symmetry and concentric zones were assumed there only to allow an exact analytic treatment of the two-zone model). In the simulations, the accretion disc is modelled as an infinite slab made of a paving of identical cubes of size H and dissipation takes place only close to the centre the cubes. The hot plasma density is uniform and characterized by a Thomson optical depth $\tau_T = n_e \sigma_T H$. The disc is also uniformly pervaded by cold dense clumps with an effective cloud optical depth τ_B. In the case of spherical clumps the total number of clumps in the cube N is given by $\tau_B = \pi N \epsilon^2$ (see MC02). In this idealization, we can afford to simulate the emission from only one paving stone by assuming that the same radiation flux that escapes to a neighbouring cube through one side, re-enters on the opposite side.

To account for expected gradients of temperature of the hot plasma and ionization parameter of the cold clouds, the cube is divided into 10 cells. Those cells are defined as the intersection between five equidistant planes that are parallel to the accretion disc and a cylinder the axis of which is normal to the slab-disc and crosses the centre of the cube (see Fig. 5). The plasma is heated only in the central cylindrical cell. The temperature in each cell is computed from the local energy balance. For a given volume averaged, ionization parameter ξ, the ionization gradient is computed from the local radiative energy density. The compactness of the active region is parametrized through $h = Z/H$, where Z is the radius of the cylinder. We assume that the cloud has a constant density, $n_{cl} = 10^{15}$ cm^{-3}, and standard (solar) abundances (see Ross & Fabian 2005, and references therein for the atomic data used in the code). The values for the cold clouds density and ionization parameters are therefore chosen within the range of values expected for accretion flows around supermassive black holes (see Appendix A). The explicit scaling with mass, and the possible relevance of our model for stellar mass black holes are discussed in Section 4.3.
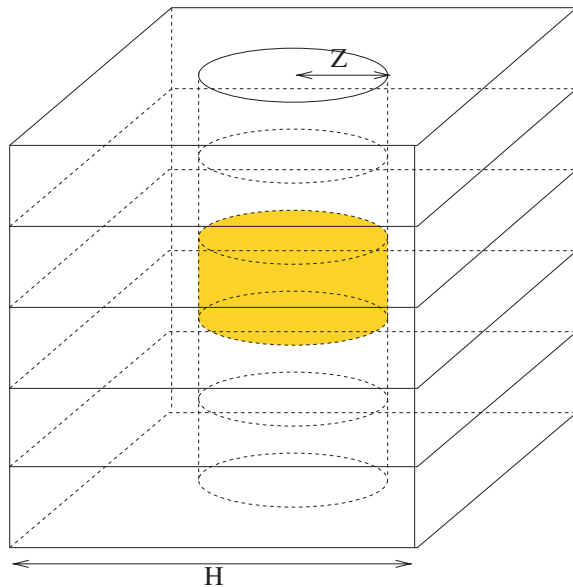

Figure 5. In numerical simulations, the disc is modelled as an infinite slab made of a paving of identical cubic regions. As shown in this sketch, each cube is itself divided into 10 cells to account for inhomogeneity. The cube is uniformly filled with hot/ionized plasma and cold clumps, but dissipation occurs only in the central (coloured) zone.

3.2 Results

Fig. 6 shows a sample of model spectra that illustrates the effects of varying τ_B from 1 to 8. The emerging spectra are clearly very complex, with prominent signatures of ionized reflection dominated by a complex of UV and soft X-ray emission lines. Strong ionization edges are observed for low ionization parameter (for high values of ξ Comptonzation has a relatively large influence on the emerging spectra and help smearing out ionization edges and lines).

As mentioned earlier, the complex geometry of our set-up will inevitably lead to multiple reflections, which in turn reduce the net albedo of the cold clumps. We have studied in detail this effect by calculating the total albedo as the ratio of incident (Comptonized) flux to the reprocessed one at energies above 0.1 and 1 keV. The results are shown in Fig. 7.

In order to quantify at least the most prominent characteristics of these spectra in the X-ray band, we have fitted them in the 2–30 keV range under XSPEC with the PEXRAV model plus a Gaussian line. During the fit the high energy cut-off energy E_c and the inclination angle were fixed at 400 keV and 30°, respectively, and the abundances were fixed to solar. Obviously, we are not interested here in the goodness of these fits, rather we want to use the fit parameters as measures of the spectral complexity. The results of the fitting procedure confirms that reflection-dominated spectra (in the sense usually implied by an observer, i.e. spectra with $R > 1$, where R is the value of the reflection fraction parameter of the PEXRAV model) can be produced with our model for the inhomogeneous disc structure. For $\tau_B = 8$ the reflection fraction is $R \sim 4$–5, even at large ionization parameters ($\xi \sim 3000$). When comparing these results with the simple toy model of Section 2, it is apparent that the PEXRAV fits indicate somewhat larger reflection fractions at small τ_B.

Below ~ 1 keV, all spectra show a distinct curvature that, when plotted as a ratio to the best-fitting power law in the 2–10 keV range, would appear as a so-called 'soft excess', indeed a ubiquitous feature in the spectra of QSOs and Seyfert galaxies (see e.g. Wilkes & Elvis 1987; Piconcelli et al. 2005). Within our model, such emission is accounted for by a plethora of emission lines produced by ionized reflection of the Comptonized continuum off the cold clumps as proposed earlier by Ballantyne, Iwasawa & Fabian (2001), Fabian et al. (2002), and more recently by Crummy et al. (2005).

Fig. 8 shows in red a detailed view of the emerging spectrum for the case $\tau_B = 3$, $\xi = 300$. By looking at the ionization structure within the gas, it is apparent that the gas is still highly ionized at the outer surface, with the dominant ions being C VII, N VIII, O IX, Ne X, Mg XI, Si XII, S XIV and Fe XVIII. However, the ionization decreases rapidly with depth, and by a Thomson depth of 1.4, the least-ionized species treated dominates for each element. Specifically they are, with their ionization potentials: C III (47.9 eV); N III (47.5 eV); O III (54.9 eV); Ne III (63.5 eV); Mg III (80.1 eV); Si IV (45.1 eV); S IV (47.3 eV) and Fe VI (99.1 eV). Within our code, the lowest absorption edge treated is thus at 45 eV. Below that energy, the only absorption treated is free–free absorption, and radiation can enter and leave the gas with ease. We should note here that in the code helium is assumed to be fully ionized (so that its only contribution is to the free electron density). However, since the least-ionized species of C, O and Si appear to be present in this particular model, some He II might be present in reality, which would produce an edge at 54.4 eV if it were included in the calculation. The four strongest low-energy emission lines are due to Si IV (11.0 eV), O III (17.6 eV), C III (21.6 eV), and O III (33.1 eV).
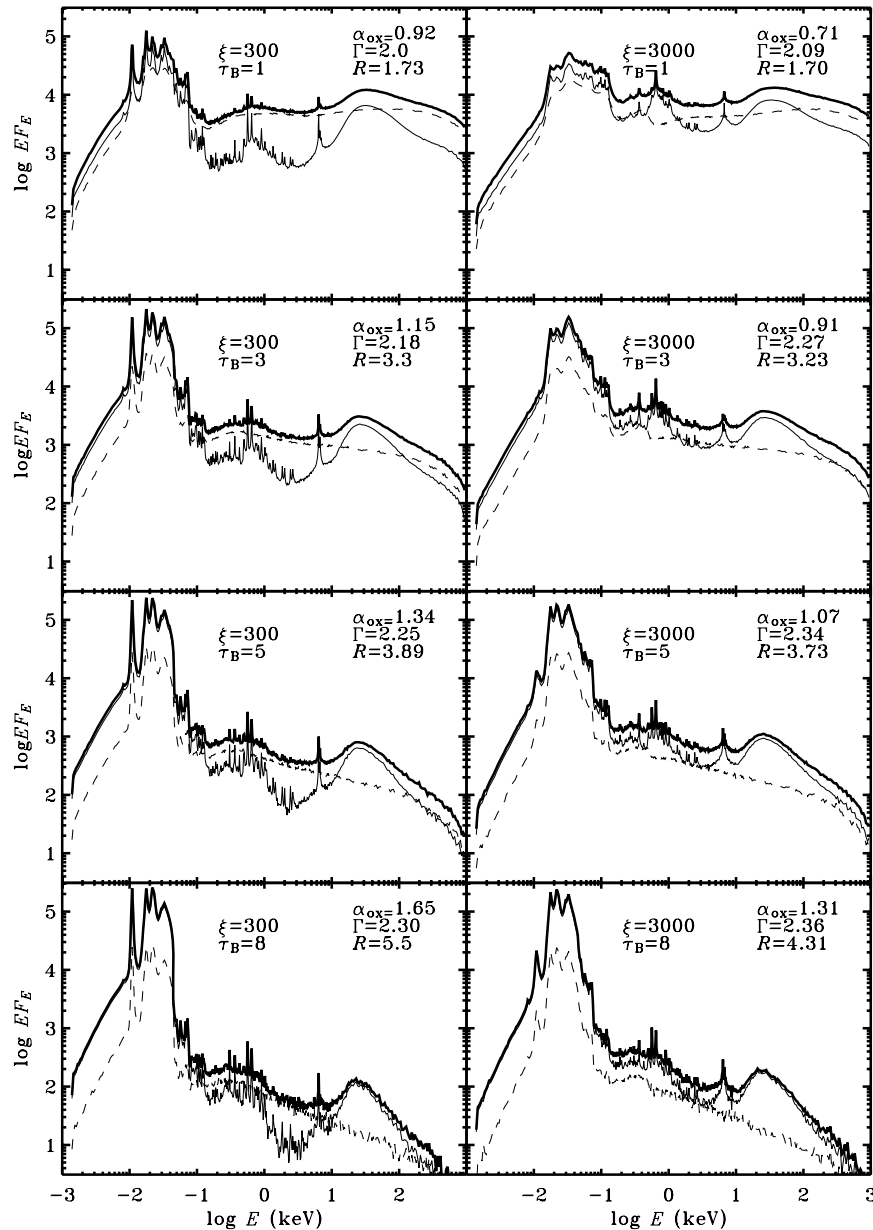
Figure 6. Effects of τ_B and ξ on the emerging spectrum. Angle averaged spectra calculated for $h = 0.1$ and $\tau_T = 1$. In each panel, are shown the corresponding τ_B and ξ as well as the best-fitting parameter R and Γ obtained when these spectra are fitted with PEXRAV in the 2–30 keV range and the optical to X-ray spectral slope α_{ox}. The thin dashed and solid curves indicate the Comptonized and the reprocessed spectra, respectively. The total spectra are shown by the thick solid curve.

The spectra shown in Fig. 6 are those emerging from a system at rest. It is obvious that, when considering the application of such a model to the inner region of an accretion disc, the effects of both the turbulent motion of the clumps and the overall rotation pattern of the two-phase disc should be taken into account (as well as cosmological redshift, obviously). Indeed, in all previous direct applications of ionized reflection models to observed data (see e.g. Fabian et al. 2002; Crummy et al. 2005), the absence of sharp emission lines both in the soft X-ray and in the Iron Kα line regions of the observed spectra was taken as an indication of extreme relativistic blurring in the inner region of the accretion disc. Without attempting to address the issue of including relativistic effects into our model in a systematic way, we show here in Fig. 8 one of our simulated spectra convolved with a relativistic disc model. The relativistic blurring

routine kdblur (Fabian & Johnstone private communication) makes use of the LAOR kernel describing relativistic effects on the spectral shape resulting from emission in an accretion disc orbiting a maximally rotating Kerr black hole (Laor 1991). Indeed, even for our relatively modest choice of blurring parameters (emissivity index = 3 and inner radius of the disc at $4.5R_g$), most of the discrete emission features in the X-ray energy range appear strongly blurred and hardly distinguishable from a curved continuum. A more extensive analysis of the strong relativistic corrections to our inhomogeneous model is beyond the scope of the present paper and will be presented elsewhere.

In terms of global spectral energy distributions, the general trend follows the expectations of the simple analytic two-zone model presented in Section 2. Strongly inhomogeneous discs with large τ_B
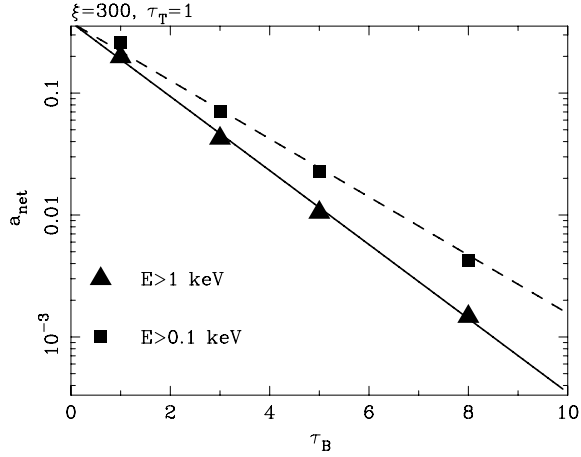
Figure 7. Solid symbols show the net albedo of the cold clumps calculated from our simulations, after multiple reflections are taken into account. With triangles we show the results obtained by considering only the reprocessed radiation above 1 keV, while squares show the results obtained by considering reprocessed radiation above 0.1 keV. Solid and dashed lines show the approximations to the analytical results by the analytic expression (4), with $a = 0.36$ (equal in both cases), $\varepsilon = \exp(-\tau_B/1.43)$ and $\varepsilon = \exp(-\tau_B/1.82)$, respectively. The solid line also shows the relation used in the analytic two-zone toy model described in Section 2.

are dominated by reflected/reprocessed UV emission. To quantify this, we have calculated the α_{ox} parameter, i.e. the slope of spectrum between 2500 Å $= 5$ eV and 2 keV: $\alpha_{ox} = -0.3838 \log(F_{2\,keV}/F_{2500})$ and the resulting values are shown in each panel of Fig. 6. We see a trend of larger α_{ox} for more complex, reflection-dominated spectra, as indeed observed (Gallo et al. 2006). At face value, α_{ox} depends quite sensitively on τ_B, thus on the degree of inhomogeneity, and can in principle represent a very useful way to tie down the general properties of the observed emission. Our model would then predict that the larger α_{ox}, i.e. the X-ray weaker a source is, the larger the reflection fraction should be, and in general, the more complex the X-ray spectra would appear. It has to be kept in mind, however, that the observed emission at 2500 Å may include a contribution from an outer, colder homogeneous accretion disc. If the extent of the in-homogeneous region of the accretion disc coincide with the region where radiation pressure dominates, the relative contribution to the optical emission at 2500 Å should depend on the accretion rate: the larger the accretion rate, the larger is the contribution from the inner inhomogeneous part we have discussed here. A full model for the dependence of α_{ox} on the source luminosity should then be made based on the combination of a inner inhomogeneous disc (Appendix A) and an outer standard, gas-pressure-dominated one.

As expected, the reflection features are weaker when h or τ_T are larger. To confirm this, we have performed two additional simulations (not shown in Fig. 6), and again fitted the emerging spectra with PEXRAV. The results as shown in Table 1. If we double the size of the inner heated region (i.e. we take $h = 0.2$), while keeping $\tau_B = 1$ constant, the measured reflection fraction, for example, drops from 1.73 to slightly less than unity.

4 DISCUSSION

The expected variability properties of the inhomogeneous flow were discussed in Section 2.1, based on the analysis of our simple two-zone toy model. Barring any additional (likely) variability associated with an intermittent heating rate, we have shown there that a
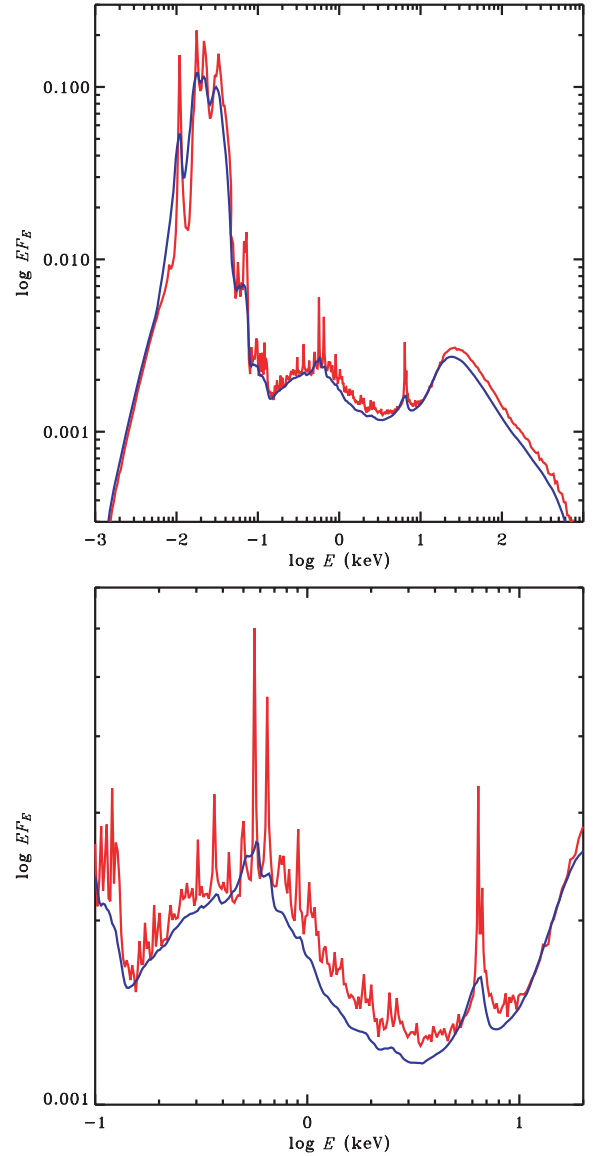

Figure 8. The spectrum obtained for $\xi = 300$ and $\tau_B = 3$ (upper curves, red online), and the same spectrum convolved with a relativistic disc model (lower curves, blue online; kdblur with $R_{in} = 4.5R_g$, $R_{out} = 100R_g$, emissivity index 3, inclination of $30°$). The top panel shows the broad-band ratio spectra (1 eV–1 MeV). The bottom panel focuses on the 0.1–30 keV range where most X-ray instruments operate.

Table 1. Spectral parameters obtained from the fit of the simulated spectra that illustrate the effects of varying the heating inhomogeneity parameter h and the Thomson optical depth of the hot phase τ_T. In all the simulations $\tau_B = 1, \xi = 300$. Γ_p and R are the PEXRAV photon index and reflection amplitude, while EW is the equivalent width in eV of the Gaussian line.

h	τ_T	Γ_p	R	EW
0.1	3	1.95	1.03	108
0.1	1	2.0	1.73	82
0.2	1	1.98	0.98	144

modest 10 per cent variation in the optical depth of the cold clouds around a mean value of $\tau_B \sim 1$–2 can produce large amplitude variations (up to 40–50 per cent) in the X-ray power-law flux with much smaller (less than 20–25 per cent) variations associated with the reflected component (see Fig. 4). This is a possible explanation for the variability pattern observed in many AGN on short (dynamical) time-scales, as discussed in more detail in Section 4.2. Of course, as in the geometrically equivalent light bending model of Miniutti & Fabian (2004), also in our model there are different regimes of variability, essentially depending on the degree of inhomogeneity of the heating rate, h, and on the optical depth of the cold clumps τ_B: when the latter is large, most of the X-ray emission *and* of the reflected radiation are hidden from view, and large amplitude variability is induced in both spectral component. On longer (thermal, viscous) time-scales, the global geometry may change substantially. Large variations of τ_B would of course correspond to substantial spectral variability. In Fig. 9 we have plotted the ratio of the spectra obtained for $\xi = 300$ and $\tau_B = 1, 5, 8$ to the $\tau_B = 3$ spectrum. Apart from the dramatic variation of the lowest absorption edge at $\sim$45 eV, and of the overall slope of the Comptonized X-ray emission (getting steeper for large τ_B), the spectra show relatively little variability despite large flux variations, especially in the X-ray energy range (0.1–30 keV). In particular, no strong soft excess below 1 keV is seen in the ratio spectrum.

4.1 Comparison with earlier theoretical works

Ballantyne et al. (2004) and Ballantyne, Turner & Young (2005) have studied X-ray reflection from inhomogeneous discs. The vertical density structure of the disc they assume is derived from a two-dimensional, time-dependent numerical radiation magnetohydrodynamical (MHD) calculation. However, their numerical set-up was such that the source of X-ray illuminating radiation was assumed to be external to the disc (a corona above it), and dynamically decoupled from it. Here, we have tried to address the different (and computationally much more challenging) situation in which there is no external hot corona (and no external energy source), but the heterogeneous, two-phase structure of the flow itself gives rise to all the observed high energy radiation spectrum. The spectroscopic studies of Ballantyne and co-workers, however, suggest that any spectrum produced by a realistic, time-varying inhomogeneous accretion disc, will pose serious interpretative challenges to planned future reverberation mapping observations. We believe that the exploration of ever more realistic model of inhomogeneous discs, possibly including both the density structure from 3-dimensional MHD simulations and the inhomogeneous heating and the detailed radiative transfer calculation similar to those we have presented here will be an extremely useful tool for the next generation of X-ray spectroscopes.

One of the basic assumptions common to many of the different inhomogeneous solutions for accretion discs (see e.g. Krolik 1998; Begelman 2002; see also the discussion in Appendix A) is that the clouds are not confined by magnetic field, but, on the contrary, that magnetic field lines connect the two phases. This implies that, for small enough clouds, each of them will be in pressure equilibrium with the surrounding hot phase. Then, the density contrast (which is a physical quantity easy to derive from numerical MHD simulations) will be approximately given by the ratio of the temperatures of the two phases, which could in principle be inferred from accurate spectroscopic studies in both soft (0.1–2 keV) and hard (5–30 keV) X-rays. In general, a more realistic density structure that takes also into account pressure equilibrium between the phases in the presence of a turbulent magnetic field should be the next step, although
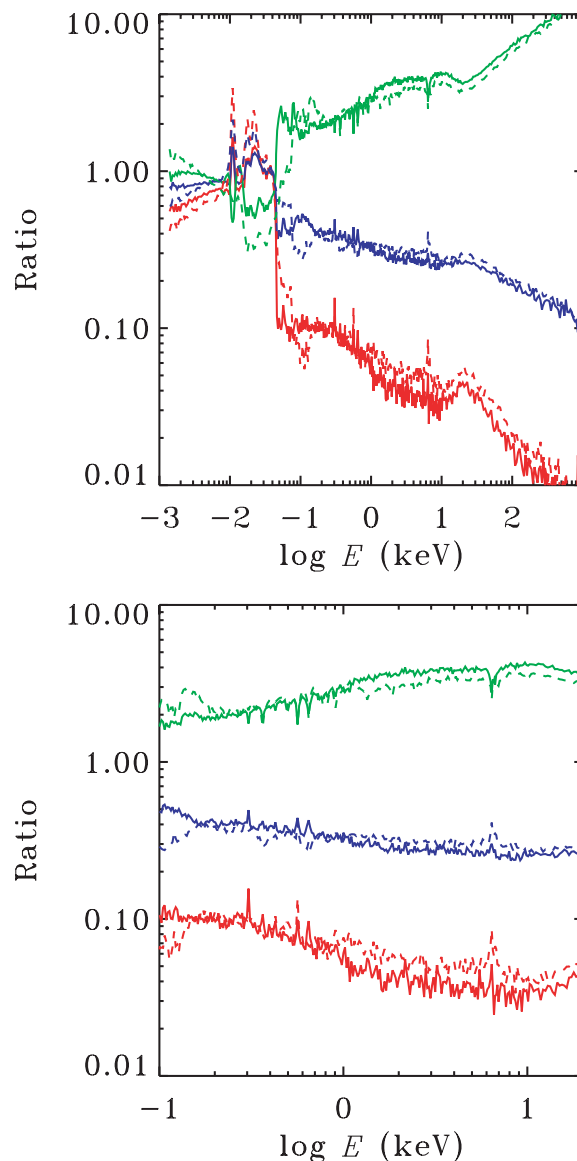

Figure 9. Ratio of the spectra obtained for $\tau_B = 1$ (upper curves, green online), $\tau_B = 5$ (middle curves, blue online) and $\tau_B = 8$ (lower curves, red online) to the spectrum for $\tau_B = 3$. The top panel shows the broad-band ratio spectra (1 eV–1 MeV). Solid lines are for $\xi = 300$, dashed lines for $\xi = 3000$. The bottom panel focuses on the 0.1–30 keV range where most X-ray instruments operate. In this limited energy band, large changes in τ_B can lead to dramatic changes in luminosity with only weak changes of the spectral shape.

an extremely complicated one, in the implementation of our inhomogeneous model.

The coupled radiative transfer code we have used in this work is probably the only one used so far capable of self-consistently calculating the radiative equilibrium between the two phases present in the innermost region of an accretion disc with such a detail. It is however very time consuming, and still limited in its wider applicability. The set-up we have discussed here, for example, assumes that all clouds are optically thick, and neglects transmission of radiation across them. If in more realistic inhomogeneous discs the cold phase is distributed among clouds spanning a range of densities, it is likely that not only reflection off optically thick clouds, but also transmission of radiation should play a role in determining the

observed spectra. In general, in these cases we can expect, for any given value of τ_B, reduced cooling and harder spectra. Moreover, the effects of both total and/or partial absorption (depending on the filling factor of the cold clumps and on their geometry) will play an important role. This interesting issue is far beyond the scope of the present paper, which is intentionally aimed at exploring a very specific physical configuration. We just note here that a pure 'absorption model' to explain the soft excess and the general X-ray spectral shapes of QSOs and AGN has been recently proposed by Gierliński & Done (2004b), and a more general and detailed study of the role of absorption has been presented in Chevallier et al. (2006).

Finally, we note that more extreme effect of bulk Comptonization which arises in the optically thick plasma in the vicinity of a black hole (Blandford & Payne 1981a,b; Payne & Blandford 1981; Niedźwiecki & Zdziarski 2006, and references therein), has been ignored. However, as in the inhomogeneous flow we envisage the great majority of the mass is concentrated in the cold phase (even though most of the volume is filled by the hot one), this effect should be safely negligible.

4.2 Comparison with observations: the case of NLS1

NLS1 galaxies, identified by the unusual narrowness of the broad component of their Hβ lines, are believed to be powered by SMBH of relatively small masses, with high accretion rates, possibly close to the Eddington level (see e.g. Pounds, Done & Osborne 1995; Boller, Brandt & Fink 1996). This fact already makes them very good candidate systems for inhomogeneous accretion. Furthermore, NLS1 galaxies have long been known to be characterized by extreme properties of their X-ray emission: a strong soft excess in the *ROSAT* soft band (0.1–2.4 keV; Boller et al. 1996); unusually steep X-ray spectra in the hard X-ray band (2–10 keV; Brandt, Mathur & Elvis 1997; Vaughan et al. 1999; Leighly 1999b); very rapid and large variability (Leighly 1999a).

Recent XMM detailed spectral studies have revealed more unusual spectral properties, most notably in the form of sharp spectral drops above 7 keV, the most extreme examples of which are found in 1H 0707−495 (Boller et al. 2002) and in IRAS 13224−3809 (Boller et al. 2003). These features are sharp and time-variable (Gallo et al. 2004). Detailed spectral modelling of these data so far suggested that either partial covering (Gallo et al. 2004; Tanaka et al. 2004) or ionized reflection-dominated discs (Fabian et al. 2002), with light bending effects (Fabian et al. 2004; Crummy et al. 2005) can explain the observed features in these as well as in other bright Seyfert galaxies (e.g. 1H 0419−577, Fabian et al. 2005; MCG-02-14-009, Porquet 2006). Within the partial covering model, variability is induced by rapid changes in the covering fraction of the absorbers. In the light bending model, instead, variability is essentially produced by a change in the distance between the X-ray emitting flares and the reprocessor very close to the black hole.

Our model falls within the family of models trying to explain the complex X-ray spectra of bright AGN with ionized reflection, though representing an alternative, specific, physically motivated, geometrical set-up for the multiphase structure of the inner regions of an accretion flow near the Eddington luminosity. In Section 2, we have already discussed the qualitative similarities between the emerging spectra expected from our inhomogeneous flow and the light bending models. Here, we would like to notice a few points concerning the partial covering model.

First, a comprehensive analysis of *XMM* data of a number of NLS1 with the partial covering model (Tanaka, Boller & Gallo 2005; see also Crummy et al. 2005) highlights the fact that the estimated tem-

perature of the soft X-ray/UV emission component (the soft excess) is very similar for objects that span more than four orders of magnitude in luminosity, as already noticed by Walter & Fink (1993); Czerny et al. (2003) and Gierliński & Done (2004b). As pointed out by Ross & Fabian (2005), the emission in the 0.2–2 keV band due to lines and bremsstrahlung in the hot surface layer of the cold medium is a signature of ionized reflection, and can appear in real data as blackbody emission, provided that the individual lines and edges are smeared by a large enough amount, so that the emerging soft excess will appear featureless (Chevallier et al. 2006; Crummy et al. 2005). Secondly, the observed rapid and strong variability of many NLS1 puts tight constraints on the maximum distance the partial coverers can possibly be at. In fact, as already discussed in detail in Gallo et al. (2004), within the partial covering model the absorber must be outflowing, have a high column density and a low ionization, which imply a kinetic energy outflow almost two orders of magnitude larger than the observed luminosity. It is more reasonable to assume that the absorber is in fact embedded within the X-ray emitter and shares with it the high rotational velocity of the inner accretion flow, as we have discussed here.

Naturally, reflection-dominated inhomogeneous flows from the vicinity of a black hole should produce strongly relativistic lines in the soft X-ray range. Previous claims of detections of such lines in the XMM spectra of two Seyfert galaxies (Mkn 766 and MCG-6-30-15, Branduardi-Raymont et al. 2001; Sako et al. 2003), have however been questioned (Ballantyne, Ross & Fabian 2002; Turner et al. 2003a) and it is yet unclear to what extent weak relativistic lines can be seen in spectra clearly dominated by (dusty) warm absorbers (see Lee et al. 2001; Turner et al. 2003a).

In a recent work, Chevallier et al. (2006) have compared absorption (and partial covering) and reflection models with the X-ray spectra of PG quasars. They reached the conclusion that absorption models seem capable of explaining some of the soft X-ray excesses, provided the absorbing clouds span a range of optical thicknesses, ionization parameters and covering fractions. On the other hand, ionized reflection models necessitate that the continuum emission is strongly suppressed, as in our inhomogeneous model or in the most extreme versions of the light bending model.

4.3 The scaling with the black hole mass

The scaling of the physical quantities most relevant for the observable characteristics of inhomogeneous accretion flows are shown explicitly in Appendix A. As the solution we describe is thought to be the final outcome of non-linear MHD instabilities in radiation-pressure-dominated discs, it is hard to predict how the parameters describing the inhomogeneity, τ_B, ϵ and h will scale with mass. This is in fact the reason why we have chosen them as free parameters of the model. However, once their values are fixed (within the range we have explored here), it is apparent that the hot phase temperature is almost independent on black hole mass (equation A13), as it was already noticed by Krolik (1998). In general, the properties of the hot phase turn out to be very insensitive to the central object mass. For example, the ratio of gas to radiation pressure in the hot phase does not depend on m, ensuring the analytic treatment presented in appendix A remains valid throughout the mass spectrum. As for the other relevant physical quantities, both cold cloud temperature and ionization parameter scale with mass as $m^{-1/4}$, while $n_{cl} \propto m^{-3/4}$: stellar mass black holes, as expected, have denser, hotter and more highly ionized clumps.

If one considered also the evaporation/condensation equilibrium between the phases (neglected here), as done by Krolik (1998), one

would infer that the cold phase covering factor should rise towards unity as the black hole mass decreases. This correspond to very large values of τ_B, for which the observational differences between an inhomogeneous flow and a more standard optically thick homogeneous disc become less and less pronounced.

Finally, there is a more general issue regarding the very existence of strong inhomogeneities in the accretion flows close to the Eddington level. In fact, the critical accretion rate above which standard Shakura–Sunyaev discs are viscously and thermally unstable depend both on the nature of the viscosity prescription and on the mass of the central accreting object (see Merloni & Nayakshin 2006). The observational fact that accretion discs in luminous black hole binaries in the so-called high state appear rather stable close to the Eddington rate, (Gierliński & Done 2004a), but unstable above it (Done, Wardziński & Gierliński 2004) has been in fact used by Merloni & Nayakshin (2006) to argue for a modified viscosity law, based on the results of an extended local stability analysis. However, if the nature of such a law is unchanged for supermassive black holes, the critical accretion rate should scale as $m^{-1/8}$. Thus, accretion flows in AGN should be unstable at the same (Eddington-scaled) accretion rates at which high state BHXRB are observed to be stable.

5 CONCLUSIONS

We have discussed the expected X-ray spectral and variability properties of black hole accretion discs at high luminosity, under the hypothesis that radiation-pressure-dominated discs are subject to violent clumping instabilities and, as a result, have a highly inhomogeneous structure. Within this picture, most of the mass is concentrated in (Thomson) optically thick clouds that fill only a small fraction of the volume, which is instead occupied by hot, optically thin Comptonizing plasma. Such a geometrical configuration was first proposed by Fabian et al. (2002) as a mean to explain the complex spectral properties of the extreme NLS1 1H 0707−495. Since then, many more bright AGN (both Seyfert and QSO) have been modelled with reflection-dominated spectra (see e.g. Crummy et al. 2005).

Here, we have presented a physically motivated model for accretion discs near the Eddington luminosity (Appendix A), and studied their radiative output by exploring the space of parameters that describe the proposed geometry (mean optical depth of the cold phase and degree of concentration of the heating source) in a simple two-zone analytical model. Moreover, we have used a sophisticated radiative transfer code to simulate the radiative equilibrium between the two phases in a self-consistent way, so that the mutual radiative feedback is fully taken into account.

The main results of our work are the following.

(i) For very inhomogeneous configurations, i.e. those which have both a large covering fraction in clouds and very concentrated dissipation, the emerging radiation can be dominated by ionized reflection.

(ii) The observed spectra are very complex, with prominent signatures of ionized reflection dominated by a plethora of UV and soft X-ray emission lines; if the blurring due to relativistic motions in the immediate vicinity of a black hole is accounted for, the soft X-ray emission will appear as a featureless continuum (a soft excess).

(iii) For a large range of parameters, even when contributing a large fraction of the hard X-ray spectrum, the reflection component is less variable than the power-law-like emission originating from the hot Comptonizing phase, in agreement with what observed in many NLS1 galaxies and bright Seyfert 1.

(iv) The reflection fraction becomes strongly variable only at very low flux levels of the hard X-ray continuum, corresponding to a configuration in which both the primary Comptonized continuum and the high energy reflection emission are essentially hidden from the observer's view.

The fact that many of these properties are common to the 'light bending' model (Miniutti & Fabian 2004) is not surprising. In fact, for a two-phase system in radiative equilibrium, the main spectral properties are determined by the radiative feedback between the hot and the cold phases. Such feedback is strongly dependent on the geometry (and on the topology) of the two phases and, in particular, on the sky covering fraction of the cold phase as seen by the hot, Comptonizing medium. Reflection dominated spectra are expected when the cold phase intercepts most of the photons coming from the hot phase.

In more general terms, one can define 'open' any geometry in which the hot, X-ray emitting plasma is photon starved. Such a geometry will produce hard X-ray spectra, little soft thermal emission and weak reflection component. On the other hand, a 'closed' geometry will instead correspond to a very large covering fraction of the cold phase, with associated strong soft emission, softer spectra and strong reflection fraction. Such a geometry corresponds, observationally, to the highly accreting black holes and is obtained via GR effects in the light bending model, while is a result of the clumpy and inhomogeneous nature of the inner unstable, radiation-pressure-dominated part of the disc in the model we have presented here.

In the end, it seems likely that a complete model for the innermost region of luminous accretion discs around black holes will involve a two-phase inhomogeneous and turbulent flow moving at relativistic speed, so that the emerging spectrum will be determined by ionized reflection off the cold phase, inverse Compton scattering in the hot phase and possibly warm absorption from an accompanying outflow, all distorted by GR effects. The model we have explored here, thus, represents a step towards our understanding of such a challenging complexity.

REFERENCES

Balbus S. A., Hawley J. F., 1991, ApJ, 376, 214
Balbus S. A., Hawley J. F., 1998, Rev. Mod. Phys. 70, 1
Ballantyne D. R., Iwasawa K., Fabian A. C., 2001, MNRAS, 323, 506
Ballantyne D. R., Ross R. R., Fabian A. C., 2002, MNRAS, 336, 867
Ballantyne D. R., Turner N. J., Blaes O., 2004, ApJ, 603, 436
Ballantyne D. R., Turner N. J., Young A. J., 2005, ApJ, 619, 1028
Begelman M. C., 2001, ApJ, 551, 897
Begelman M. C., 2002, ApJ, 568, L97
Belloni T., 2004, Nucl. Phys. B: Proc. Suppl., 132, 337
Blaes O., Socrates A., 2001, ApJ, 553, 987
Blaes O., Socrates A., 2003, ApJ, 596, 509
Blandford R. D., Payne D. G., 1981a, MNRAS, 194, 1033

Blandford R. D., Payne D. G., 1981b, MNRAS, 194, 1041

Boller T., Brandt W. N., Fink H., 1996, A&A, 305, 53

Boller T. et al., 2002, MNRAS, 329, L1

Boller T., Tanaka Y., Fabian A. C., Brandt W. N., Gallo L., Anabuki N., Haba Y., Vaughan S., 2003, MNRAS, 343, L89

Brandt W. N., Mathur S., Elvis M., 1997, MNRAS, 285, L25

Branduardi-Raymont G., Sako M., Kahn S., Brinkman A. C., Kaastra J. S., Page M. J., 2001, A&A, 365, L140

Celotti A., Fabian A. C., Rees M. J., 1992, MNRAS, 255, 419

Chevallier L., Collin S., Dumont A.-M., Czerny B., Mouchet M., Gonçalves A. C., Goosmann R., 2006, A&A, 449, 493

Collin-Souffrin S., Czerny B., Dumont A.-M., Życki P. T., 1996, A&A, 314, 393

Crummy J., Fabian A. C., Gallo L., Ross R. R., 2006, MNRAS, 365, 1067

Czerny B., Nikolajuk M., Różańska A., Dumont A.-M., Loska Z., Życki P. T., 2003, A&A, 412, 317

Davis S., Blaes O., Turner N., Socrates A., 2004, In Richards G. T., Hall P. B., eds, ASP Conf. Ser. 311, AGN Physics with the Sloan Digital Sky Survey. Astron. Soc. Pac., San Francisco, p. 135

Done C., Wardziński G., Gierliński M., 2004, MNRAS, 349, 393

Elvis M., Risaliti G., Zamorani G., 2002, ApJ, 565, L75

Fabian A. C., Iwasawa, K., 1999, MNRAS, 303, L34

Fabian A. C., Ballantyne D. R., Merloni A., Vaughan S., Iwasawa K., Boller Th., 2002, MNRAS, 331, L35

Fabian A. C., Miniutti G., Gallo L., Boller Th., Tanaka Y., Vaughan S., Ross R. R., 2004, 353, 1071

Fabian A. C., Miniutti G., Iwasawa K., Ross R. R., 2005, MNRAS, 361, 795

Gallo L., Tanaka Y., Boller T., Fabian A. C., Vaughan S., Brandt W. N., 2004, MNRAS, 353, 1064

Gallo L., 2006, MNRAS, 368, 479

Gammie C., 1998, MNRAS, 297, 929

Ghisellini G., Haardt F., Matt G., 1994, MNRAS, 267, 743

Gierliński M., Done C., 2004a, 347, 885

Gierliński M., Done C., 2004b, 349, L7

Guilbert P. W., Rees M. J., 1988, MNRAS, 233, 475

Kuncic Z., Celotti A., Rees M. J., 1997, MNRAS, 284, 717

Krolik J. H., 1998, ApJ, 498, L13

Krolik J. H., 1999, in Poutanen J., Svensson R., eds, ASP Conf. Ser. Vol. 161, High Energy Processes in Accreting Black Holes. Astron. Soc. Pac., San Francisco, p. 315

Laor A., 1990, MNRAS, 246, 369

Laor A., 1991, ApJ, 376, 90

Lee J. C., Ogle P. M., Canizares C. R., Marshall H. L., Schulz N. S., Morales R., Fabian A. C., Iwasawa K., 2001, ApJ, 554, L13

Leighly K. M., 1999a, ApJS, 125, 297

Leighly K. M., 1999b, ApJS, 125, 317

Lightman A. P., Eardley D. M., 1974, ApJ, 187, L1

Lightman A. P., Zdziarski A. A., 1987, ApJ, 319, 643

Magdziarz P., Zdziarski A. A., 1995, MNRAS, 273, 837

Malkan M. A., 1983, ApJ, 268, 582

Malzac J., 2001, MNRAS, 325, 1625

Malzac J., Celotti A., 2002, MNRAS, 335, 23 (MC02)

Malzac J., Jourdain E., 2000, A&A, 359, 843

Malzac J., Dumont A. M., Mouchet M., 2005, A&A, 430, 761

Marconi A., Risaliti G., Gilli R., Hunt L. K., Maiolino R., Salvati M., 2004, MNRAS, 351, 169

McClintock J. E., Remillard R. A., 2006, in Lewin W. H. G., van der Klis M., eds, Compact Stellar X-Ray Sources. Cambridge Univ. Press, Cambridge, in press, preprint (astro-ph/0306213)

Merloni A., Nayakshin S. 2006, MNRAS, submitted, preprint (astro-ph/0603159)

Merloni A., Rudnick G., Di Matteo T., 2004, MNRAS, 354, L73

Miniutti G., Fabian A. C., 2004, MNRAS, 349, 1435

Miniutti G., Fabian A. C., Goyder R., Lasenby A. N., 2003, MNRAS, 344, L22

Miniutti G., Fabian A. C., Miller J. M., 2004, MNRAS, 351, 466

Niedźwiecki A., Zdziarski A., 2006, MNRAS, 365, 606

Payne D. G., Blandford R. D., 1981, MNRAS, 196, 781

Piconcelli E., Jimenez-Bailón E., Guainazzi M., Schartel N., Rodríguez-Pascual P. M., Santos-Lleó M., 2005, A&A, 432, 15

Porquet D., 2006, A&A, 445, L5

Pounds K. A., Done C., Osborne J. P., 1995, MNRAS, 325, 1625

Ross R. R., Fabian A. C., 1993, MNRAS, 261, 74

Ross R. R., Fabian A. C., 2005, MNRAS, 358, 211

Ross R. R., Fabian A. C., Ballantyne D. R., 2002, MNRAS, 336, 315

Rossi S., Homan J., Miller J. M., Belloni T., 2005, MNRAS, 360, 763

Sako M. et al., 2003, ApJ, 596, 114

Shakura N. I., Sunyaev R. A., 1973, A&A, 24, 337

Shakura N. I., Sunyaev R. A., 1976, MNRAS, 175, 613

Shang Z. et al., 2005, ApJ, 619, 41

Tanaka Y., Boller T., Gallo L., Keil R., Ueda Y., 2004, PASJ, 56, 9

Tanaka Y., Boller T., Gallo L., 2005, in Merloni A., Nayakshin S., Sunyaev R., eds, Growing Black Holes: Accretion in a Cosmological Context. Springer-Verlag series of 'ESO Astrophysics Symposia', p. 290

Turner N. J., 2004, ApJ, 605, L45

Turner N. J., Stone J. M., Sano T., 2002, ApJ, 566, 148

Turner A. K., Fabian A. C., Vaughan S., Lee J. C., 2003a, MNRAS, 346, 833

Turner A. K., Stone J. M., Krolik J. H., Sano T., 2003b, ApJ, 593, 992

Turner N. J., Blaes O., Socrates A., Begelman M. C., 2005, ApJ, 624, 267

Vaughan S., Reeves J., Warwick R., Edelson R., 1999, MNRAS, 309, 113

Walter R., Fink H. H., 1993, A&A, 274, 105

Wardziński G., Zdziarski A. A., 2000, MNRAS, 314, 183

Wilkes B. J., Elvis M., 1987, ApJ, 323, 243

Yu Q., Tremaine S., 2002, MNRAS, 335, 965

Zdziarski A. A., 1999, In Poutanen J., Svensson R., eds, ASP Conf. Ser. Vol. 161, High Energy Processes in Accreting Black Holes. Astron. Soc. Pac., San Francisco, p. 16

Zdziarski A. A., Lubiński P., Smith D. A., 1999, MNRAS, 303, L11

APPENDIX A: A FULL INHOMOGENEOUS ACCRETION DISC MODEL

We derive here a full accretion disc model in which the inhomogeneous structure is introduced through the parameters τ_B, τ_T, Θ, ϵ, h, as discussed in the paper. We will follow closely the approach of Krolik (1998) that studied analytically the overall equilibrium of a clumpy two-phase accretion disc under the hypothesis that the cold clumps are magnetically connected to the hot phase. This configuration turns out to be both thermally and viscously stable. Its energy flow is more complicated than that of standard uniform disc as exemplified by the flow chart of fig. 1 of Krolik (1999). The hot phase heat comes either from magnetic field reconnection and thermalization of cloud random motions (either due to drag or inelastic collisions), while the cold phase is heated either through cloud–cloud collisions and through reprocessing of the hot phase radiation. In order to allow a simplified treatment of the radiative coupling between the phases, both in our toy model (Section 2) and in the radiative transfer simulations (Section 3) we have neglected internal dissipation in the clouds due to their inelastic collisions, and focussed only on their heating by absorption of radiation emitted in the hot phase. We will keep this assumption here, equivalent to setting to zero the term α_C in Krolik (1998).

We begin by expressing the angular momentum conservation equation in terms of the cold clumps velocity dispersion σ_{cl}. Here we adopt the customary α viscosity prescription of Shakura & Sunyaev (1973), independently of the details on how exactly the stress is produced (see Krolik 1999, for a discussion). In the following, we will indicate the accretion disc radius in units of the Schwarzschild radius as r, and the accretion rate in terms of the dimensionless quantity $\dot{m} = \epsilon_{rad}\dot{M}c^2/L_{Edd}$ with the radiative efficiency $\epsilon_{rad} = 1/12$ fixed to its Newtonian value, as appropriate for the inner boundary condition

we have adopted. We have

$$\alpha \sigma_{cl}^2 = \frac{\Omega \dot{M} J(r)}{3\pi \Sigma}, \tag{A1}$$

where Ω is the Keplerian angular velocity, $\Sigma = 2\rho H$ and the function $J(r) = (1 - \sqrt{r_{in}/r})$, with $r_{in} = 3$, describes the Newtonian approximation of the no-torque at the inner boundary condition for a disc around a Schwarzschild black hole. The velocity dispersion of the clouds can be expressed in terms of the hot phase sound speed, $c_{s,h}$:

$$\sigma_{cl} \equiv \mathcal{M} c_{s,h} \simeq 3.2 \times 10^8 \Theta_{-1}^{1/2} \mathcal{M}, \tag{A2}$$

where is the temperature of the hot phase in units of $m_e c^2/k$. As discussed in Krolik (1998), if the mean separation between the clumps is of the order of the disc scaleheight, the difference in the potential between neighbouring clumps is then big enough to stir them at $\mathcal{M} \sim 1$. In fact, within our simple geometrical model of Section 2 and for small enough clumps, we can estimate the mean clump separation in units of H as $\sim 0.2 \, \tau_B^{-1/3} \epsilon_{-1}^{2/3}$.

The angular momentum conservation equation (A1) can then be cast as a constraint on the total (cold plus hot phases) average Thomson optical depth of the inhomogeneous disc, $\tau_{tot} = \kappa \Sigma/2$, with κ electron scattering opacity, i.e. the optical depth the disc would have if it was homogeneous:

$$\tau_{tot} = 2.6 \times 10^3 \alpha^{-1} r^{-3/2} \dot{m} J(r) \mathcal{M}^{-2} \Theta_{-1}^{-1}. \tag{A3}$$

Let us now discuss the hydrostatic equilibrium of the disc. For the hot phase, assuming that gas pressure dominates over radiation pressure, the disc scaleheight is given by

$$H \simeq 1.4 \times 10^{10} m_7 r^{3/2} \Theta_{-1}^{1/2}. \tag{A4}$$

The cold clumps, obviously, will be distributed over a scaleheight of the order of $\mathcal{M} H$.

We can now verify that indeed our assumption about the pressure dominance in the hot phase is justified. The gas pressure is given by

$$P_{gas,h} = 2\rho_h k T_{hot} \simeq 1.9 \times 10^7 m_7^{-1} r^{-3/2} \Theta_{-1}^{1/2} \tau_T \text{ dyne}, \tag{A5}$$

while for the radiation pressure we have

$$P_{rad,h} = \frac{\tau_T Q}{3c} \simeq 1.8 \times 10^8 m_7^{-1} r^{-3} \dot{m}_{-1} J(r) \tau_T \text{ dyne}, \tag{A6}$$

where Q is the disc dissipation rate per unit area. Their ratio is then given by

$$\frac{P_{rad,h}}{P_{gas,h}} \simeq 5.8 r^{-3/2} \dot{m}_{-1} J(r) \Theta_{-1}^{-1/2} < 0.11 \dot{m}_{-1} \Theta_{-1}^{-1/2}, \tag{A7}$$

where the inequality in the above expression comes from taking the maximum of the radial function $r^{-3/2} J(r)$ (at $r = 16/3 \simeq 5.33$). So our assumption is justified for sub-Eddington discs.

The radiative properties of the system will be in general a function of the density, temperature, total number and geometry of the cold clouds. We can estimate the cold clump temperature under the zeroth-order assumption that they will reradiate thermally all the radiation coming from the hot phase. Consequently, we can write $Q/(ch^2) = 4\sigma_B T_{bb}/c$, where σ_B is the Stefan–Boltzmann constant, and we have allowed for inhomogeneous heating by introducing the parameter h, the size of the heated region in units of the disc scaleheight (see Section 2). Thus we get, for the cold cloud temperature:

$$k T_{bb} \simeq 1.1 \times 10^2 m_7^{-1/4} r^{-3/4} \left(\frac{1-a}{0.64}\right)^{1/4}$$
$$\times [\dot{m}_{-1} J(r)]^{1/4} h_{-1}^{-1/2} \text{ eV}. \tag{A8}$$

Then, assuming pressure balance between the clouds and the hot ambient phase we get, for the cloud density:

$$n_{cl} \simeq 1.0 \times 10^{17} m_7^{-3/4} r^{-3/4} [(1-a)\dot{m}_{-1} J(r)]^{-1/4}$$
$$\times h_{-1}^{1/2} \tau_T \Theta_{-1}^{1/2} \text{ cm}^{-3}. \tag{A9}$$

Neglecting the weak dependence on the albedo a, the typical ionization parameter, in units of erg cm s^{-1}, is given by

$$\xi \simeq 1.3 \times 10^5 m_7^{-1/4} r^{-9/4} [\dot{m}_{-1} J(r)]^{5/4} h_{-1}^{-5/2} \tau_T^{-1} \Theta_{-1}^{-1/2}. \tag{A10}$$

For the fiducial values of the parameters we are discussing here, ξ attains a maximum value of about 10^3, close to the radius of maximal dissipation in the disc. Also as expected, the strongest dependence is on the geometrical factor h, as the ionization state of the cloud surfaces will be most sensitive to the heating inhomogeneity.

The cold clouds filling factor is given by $f = (4/3)\epsilon \tau_B$, and the total density in the disc is then

$$n_{tot} = f n_{cl} + (1-f) n_h = n_{cl} \left[f + (1-f)\frac{T_{bb}}{T_{hot}} \right] \approx \frac{4}{3}\epsilon \tau_B n_{cl}. \tag{A11}$$

It is now possible to close the disc structure equations and find a relationship between the model free parameters (τ_B, τ_T, Θ, ϵ, h) and the physical parameters of the standard accretion disc solutions (mass, accretion rate, viscosity, etc.). In order to do so, we equate the total disc optical depth, dominated by the cold phase, $\sigma_T n_{tot} H$ to the expression in equation (A3). Finally, we obtain

$$\tau_B \tau_T \Theta_{-1}^2 \epsilon_{-1} h_{-1}^{1/2} \simeq 22 r^{-9/4} [\dot{m}_{-1} J(r)]^{5/4} m_7^{-1/4} \alpha^{-1} \mathcal{M}^{-2}. \tag{A12}$$

So far, we have neglected the condensation/evaporation equilibrium between the cold and the hot phase. If we introduce the relationship between the typical cloud size and the hot phase temperature and density, as derived by Krolik (1998, equation 5), we obtain the following expression for the hot phase temperature:

$$\Theta \simeq 0.36 \alpha^{-2/7} m_7^{-1/14} r^{-9/14} [\dot{m}_{-1} J(r)]^{5/14}$$
$$\times \mathcal{M}^{-4/7} \tau_B^{-2/7} h_{-1}^{1/7}, \tag{A13}$$

almost independent on black hole mass and only weakly dependent on accretion rate.

To conclude, it is interesting to notice that we have obtained a self-consistent solution for the inner radii (i.e. those where radiation pressure is supposed to dominate) of supermassive black holes accreting at a few tenths of the Eddington rate for our fiducial parameters, i.e. both τ_T and τ_B of the order unity and h, ϵ, Θ all of the order 10^{-1}. In both Sections 2 and 3 we have explored in detail the radiative equilibrium and the expected spectral and variability signature of an accretion disc in which all the above parameters are either fixed at, or allowed to vary around, these fiducial numbers. The fact that they indeed correspond to the right values for a full accretion disc model as we have outlined here is indeed a very encouraging result.

APPENDIX B: ANALYTICAL ESTIMATES OF THE EMERGING LUMINOSITIES FOR THE TWO-ZONE MODEL

For each zone, the escaping luminosity is related to the internal energy through the escape probability (Lightman & Zdziarski 1987):

$$\dot{P} = \left(\frac{L}{U}\right)\left(\frac{H}{c}\right), \tag{B1}$$

which depends on the geometry, sources distribution, optical depth and energy. We consistently indicate as $\dot{P}_C{}^j$, $\dot{P}_{UV}{}^j$, $\dot{P}_R{}^j$, the escape probability for Comptonized, soft and reflected radiation, with $j =$ i, o for the inner and outer zone, respectively, and will use the analytical approximation to $\dot{P}$ given in the appendix of MC02. For the inner zone we assume for the escape probability the analytic formula appropriate for a spherical geometry with central isotropic injection (equation A3 of MC02). For the outer zone, a central isotropic injection in spherical geometry is appropriate as long as $h \ll 1$, while for $h \longrightarrow 1$ a slab geometry should be more appropriate. Thus, we employ an interpolating expression for the intermediate cases.

Also, we should include a term that depends on the *average* fraction $\bar{K}$ of the emerging luminosity from the outer zone that re-enters the inner one. This is computed as follows. Consider a shell of width $\mathrm{d}r$ located at a distance r from the centre, with $r > h$. The solid angle (divided by 2π) subtended by the inner zone as seen from the shell is $K(r) \equiv \Delta\Omega/2\pi = 1 - \sqrt{1 - (h/r)^2}$. Then we can define

$$\bar{K} = \frac{1}{1-h} \int_h^1 K(r)\,\mathrm{d}r = 1 - \frac{\mathcal{I}}{1-h}, \qquad (B2)$$

where the integral is evaluated to

$$\mathcal{I} = \sqrt{1 - h^2} + h \arcsin h - h\left(\frac{\pi}{2}\right). \qquad (B3)$$

As we assume uniform density for the hot and cold phase, we have that the optical depths in the two zones are simply given by $\tau_T^i = h\tau_T$, $\tau_T^o = (1-h)\tau_T$; and analogously for τ_B.

Inner zone: The soft luminosity in the hot phase is produced by the clouds through absorption and reprocessing of the Comptonized and reflected radiation and disappears through escape or Comptonization, additionally, a fraction of the soft luminosity emitted by the outer zone re-enters the inner zone. Thus, the radiative equilibrium balance for U_{UV}^i reads

$$(\dot{P}_{UV}{}^i + \tau_T^i)U_{UV}^i = \tau_B^i(1-a)U_C^i + \tau_B^i(1-a_R)U_R^i \\ + (\bar{K})\dot{P}_{UV}{}^o U_{UV}^o, \qquad (B4)$$

where a and a_R are the clouds energy and angle integrated albedo for a Comptonized and a reflection spectrum, respectively.

Similarly, the reflected radiation is formed through reflection of the Comptonized and reflected radiation on the clouds, and disappears via escape, Comptonization in the hot plasma and absorption by the clouds:

$$\left[\dot{P}_R{}^i + \tau_T^i + \tau_B^i(1-a_R)\right]U_R^i = \tau_B^i a U_C^i + \bar{K}\dot{P}_R{}^o U_R^o. \qquad (B5)$$

The fraction of the internal energy in the form of Comptonized radiation has as main source the power dissipated in the hot plasma but also the Comptonized soft and reflected radiation; the sink term is due to escape, absorption and reflection by the clouds:

$$\left(\dot{P}_C{}^i + \tau_B^i\right)U_C^i = \frac{L_h H}{c} + \tau_T^i U_{UV}^i + \tau_T^i U_R^i + \bar{K}\dot{P}_C{}^o U_C^o. \qquad (B6)$$

Outer zone: Similarly, we can write the equations for the radiative equilibrium in the outer zone, considering that all the luminosities emerging from the inner zone have to enter the outer zone:

$$\left(\dot{P}_{UV}{}^o + \tau_T^o\right)U_{UV}^o = \tau_B^o(1-a)U_C^o + \tau_B^o(1-a_R)U_R^o \\ + \dot{P}_{UV}{}^i U_{UV}^i, \qquad (B7)$$

$$\left[\dot{P}_R{}^o + \tau_T^o + \tau_B^o(1-a_R)\right]U_R^o = \tau_B^o a U_C^o + \dot{P}_R{}^i U_R^i, \qquad (B8)$$

$$\left(\dot{P}_C{}^o + \tau_B^o\right)U_C^o = \tau_T^o U_{UV}^o + \tau_T^o U_R^o + \dot{P}_C{}^i U_C^i. \qquad (B9)$$

The above system of six equation in the six unknown (U_i^j, with $j =$ i, o and $i =$ C, R, UV) can be solved analytically, and the three escaping luminosities finally computed through equation (B1).

An estimate for the observed reflection coefficient can be directly obtained from

$$R \sim \frac{L_R^o}{a_{net} L_X^o}, \qquad (B10)$$

where L_X is the Comptonized luminosity above $1\,\mathrm{keV}$. For the net albedo (accounting for multiple reflections), a_{net}, we use the expression in equation (4), derived from a calibration with the numerical simulations, as discussed in Section 2. This formula corresponds to an angle averaged reference slab-reflection spectrum. Actually, the reflection coefficient also depends on the assumed inclination angle for the infinite slab model (see e.g. PEXRAV model in XSPEC, Magdziarz & Zdziarski 1995). Equation (A10) could be corrected for this, for example, by dividing it by the angular factor given by equation (2) of Ghisellini, Haardt & Matt (1994). However, for the relatively low inclination angles usually assumed in spectral fits, the correction is small and, for simplicity, we will neglect it.

This paper has been typeset from a TEX/LATEX file prepared by the author.